UV photochemistry of carboxylic acids at the air-sea boundary: A relevant source of glyoxal and other oxygenated VOC in the marine atmosphere

R. Chiu, L. Tinel, L. Gonzalez, R. Ciuraru, F. Bernard, C. George, R. Volkamer

AGU PUBLICATIONS

Geophysical Research Letters

RESEARCH LETTER
10.1002/2016GL071240

Key Points:
- UV irradiation of carboxylic acids is a source for unsaturated OVOCs, e.g., alkenals
- Glyoxal and aldehydes form as secondary products from gas phase ozonolysis of alkenals
- The mechanism explains why ambient glyoxal fluxes are directed into the ocean and adds a potentially significant marine source of OVOC

Supporting Information:
- Supporting Information S1

Correspondence to:
R. Volkamer and C. George,
Rainer.Volkamer@colorado.edu;
Christian.George@ircelyon.univ-lyon1.fr

Citation:
Chiu, R., L. Tinel, L. Gonzalez, R. Ciuraru, F. Bernard, C. George, and R. Volkamer (2017), UV photochemistry of carboxylic acids at the air-sea boundary: A relevant source of glyoxal and other oxygenated VOC in the marine atmosphere, *Geophys. Res. Lett.*, *44*, 1079–1087, doi:10.1002/2016GL071240.

Received 20 SEP 2016
Accepted 15 DEC 2016
Accepted article online 17 DEC 2016
Published online 18 JAN 2017

UV photochemistry of carboxylic acids at the air-sea boundary: A relevant source of glyoxal and other oxygenated VOC in the marine atmosphere

R. Chiu[1,2], L. Tinel[3], L. Gonzalez[1,2], R. Ciuraru[3,4], F. Bernard[3,5], C. George[3], and R. Volkamer[1,2]

[1]Department of Chemistry and Biochemistry, University of Colorado Boulder, Boulder, Colorado, USA, [2]CIRES, University of Colorado Boulder, Boulder, Colorado, USA, [3]Université Lyon, Université Claude Bernard Lyon 1, CNRS, IRCELYON, Villeurbanne, France, [4]Now at UMR ECOSYS, INRA, AgroParisTech, Université Paris-Saclay, Thiverval-Grignon, France, [5]Now at Chemical Sciences Division, Earth System Research Laboratory, National Oceanic and Atmospheric Administration, Boulder, Colorado, USA

Abstract Photochemistry plays an important role in marine dissolved organic carbon (DOC) degradation, but the mechanisms that convert DOC into volatile organic compounds (VOCs) remain poorly understood. We irradiated carboxylic acids (C_7–C_9) on a simulated ocean surface with UV light (<320 nm) in a photochemical flow reactor and transferred the VOC products into a dark ozone reactor. Glyoxal was detected as a secondary product from heptanoic, octanoic, and nonanoic acid (NA) films, but not from octanol. Primary glyoxal emissions were not observed, nor was glyoxal formed in the absence of ozone. Addition of a photosensitizer had no noticeable effect. The concurrent detection of heptanal in the NA system suggests that the ozonolysis of 2-nonenal is the primary chemical mechanism that produces glyoxal. This source can potentially sustain tens of parts per trillion by volume (pptv) glyoxal over oceans, and helps to explain why glyoxal fluxes in marine air are directed from the atmosphere into the ocean.

1. Introduction

Oceans are a major reservoir of dissolved organic carbon (DOC), but the processes by which DOC is liberated to the gas phase remain poorly understood. In the past, it was thought that surfactants in the sea surface microlayer (SML) acted primarily as physical barriers that inhibited air-sea exchange of organic gases [*Liss and Duce*, 1997]. In waters near the surface, DOC is injected into the atmosphere as sea spray aerosol [*O'Dowd et al.*, 2004; *Quinn et al.*, 2014]. Photochemistry in the surface ocean plays a key role in determining the sources of primary marine aerosol (PMA) [*Long et al.*, 2014]. Recent isotope data show that submicron water-soluble organic aerosols over the Pacific Ocean derive around 40–90% of their carbon from oceanic DOC [*Turekian et al.*, 2003; *Miyazaki et al.*, 2016]. PMA is enriched by a factor of 133 ± 10 compared to the DOC content of seawater and deemed responsible for a primary organic aerosol source of 8–50 Tg C yr^{-1} [*Spracklen et al.*, 2008; *Gantt et al.*, 2009; *Kieber et al.*, 2016]. Photochemical breakdown of DOC forms carbon monoxide, carbonyl compounds, and α-keto acids in subsurface waters [*Kieber et al.*, 1989, 1990, 2016; *Mopper et al.*, 1991; *Moran and Zepp*, 1997] and is responsible for a marine source of 31 Tg C yr^{-1} acetaldehyde to the atmosphere [*Millet et al.*, 2010]. Glyoxal, the simplest α-dicarbonyl compound, is widespread over oceans [*Wittrock et al.*, 2006; *Lerot et al.*, 2010]. Its brief atmospheric lifetime (~2–4 h) limits transport from terrestrial sources and requires production from local sources to explain significant concentrations over the remote oceans [*Sinreich et al.*, 2010; *Mahajan et al.*, 2014; *Lawson et al.*, 2015; *Volkamer et al.*, 2015]. DOC photochemistry in subsurface waters cannot explain the missing marine source either, due to the high glyoxal solubility ($H_{eff} = 4.2 \times 10^5$ M atm^{-1}) [*Ip et al.*, 2009]. Eddy covariance flux measurements indicate that the ocean is a net sink for glyoxal during most of the day [*Coburn et al.*, 2014], raising questions about possible precursors. Atmospheric models currently cannot explain glyoxal over oceans for lack of a source mechanism but estimate 20 Tg yr^{-1} glyoxal based on satellite observations [*Myriokefalitakis et al.*, 2008], which is probably a lower limit [*Lerot et al.*, 2010]. Glyoxal forms oxalic acid in marine clouds [*Rinaldi et al.*, 2011], and uptake is enhanced by salts in aqueous aerosols (salting in) [*Kampf et al.*, 2013; *Waxman et al.*, 2015] to form secondary organic aerosol [*Waxman et al.*, 2013; *Knote et al.*, 2014]. Oleic acid is an animal and vegetable fat that has been observed in the ocean [*Zahardis and Petrucci*, 2007]. Other carboxylic acids are also widespread in marine aerosols [*Hawkins et al.*, 2010; *Kawamura et al.*, 2012; *Miyazaki et al.*, 2016].

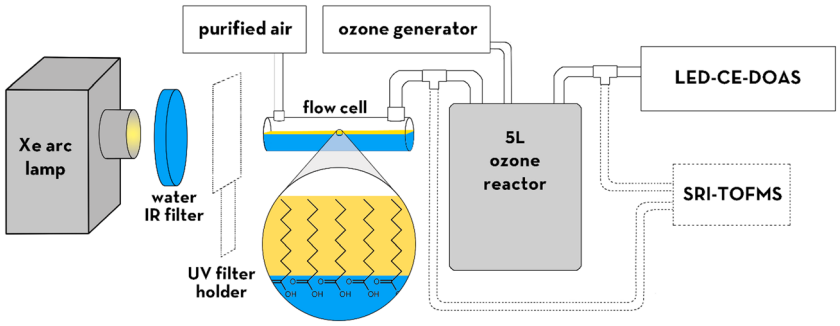

Figure 1. Diagram of the experimental setup. The xenon arc lamp, IR filter, flow cell, ozone reactor, and LED-CE-DOAS were employed in all experiments. Dashed components indicate components that were not used in all experiments.

The reaction of ozone with oleic acid at a simulated ocean surface was found a source for oxygenated volatile organic compounds (OVOCs) including glyoxal [*Mopper et al*., 1991; *Zhou et al*., 2014], but the surface flux cannot explain field observations of glyoxal over oceans [*Sinreich et al*., 2010; *Coburn et al*., 2014]. Nonanoic acid (NA) forms from the oxidation of oleic acid [*King et al*., 2009] and has been used as a proxy for SML carboxylic acid chemistry more generally. Photosensitized interfacial chemistry of NA is a source of nonenal and other OVOC [*Ciuraru et al*., 2015], but it is unclear which nonenal isomer forms, and whether it acts as a precursor for glyoxal. Here we present a series of laboratory experiments investigating whether the irradiation of carboxylic acids at a simulated ocean surface is a source of glyoxal, in the presence and absence of a photosensitizer.

2. Experimental Setup

The experimental setup is shown in the schematic in Figure 1. A cylindrical quartz cuvette with a path length of 100 mm and an internal diameter of 19 mm was used as a photoreactor (internal volume 28 mL). A xenon arc lamp was placed at one end of the photoreactor flow cell. A 5 cm quartz cuvette filled with water was placed between the xenon arc lamp and the photoreactor to filter out infrared light. A filter holder was placed between the infrared filter and the photoreactor so that an optional UV filter could be introduced for some experiments. All tubing used in the setup was made of Teflon. The inlet of the photoreactor was connected to a supply of purified air. The outlet of the photoreactor was connected to an aluminum foil-wrapped 5 L glass bottle which was used as an ozone reaction chamber. The aluminum foil ensured that only ozonolysis took place inside the ozone reactor, rather than photolysis from stray UV light from the rest of the setup. A separate piece of tubing was used to feed ozone into the ozone reactor from an ozone generator. The outlet from the ozone reactor was connected to an aerosol filter, and from there to a Light Emitting Diode Cavity Enhanced Differential Optical Absorption Spectroscopy (LED-CE-DOAS) instrument. During selected experiments a selective reagent ionization time of flight mass spectrometer (SRI-TOFMS) was connected.

2.1. Aqueous Phase

In each experiment, 14 mL of water was injected into the photoreactor, filling half of its volume. The pH was varied between 1.2 (by adding HCl), 4 (potassium biphthalate, KHP), and 7 (pH buffer solution, Sigma Aldrich), but pH effects were found to be small. The ionic strength of the aqueous phase was varied systematically from absence of salts to seawater concentrations by adding 1 mol L^{-1} NaCl, 1 mmol L^{-1} NaBr, and 10 μmol L^{-1} NaI (Sigma Aldrich, ≥99% pure). Table S1 in the supporting information provides further details about the combination of freshwater, saltwater and pH conditions investigated. In two experiments, a commercial KHP pH 4 buffer solution was used as the aqueous phase. KHP absorbs strongly at UV wavelengths and effectively acts as an aqueous phase UV filter (Figure S1). In three experiments using NA as organic phase, the aqueous phase was a solution of 40 mg L^{-1} humic acid (Sigma Aldrich) used as photosensitizers.

2.2. Organic Phase

Three carboxylic acids were investigated: nonanoic, octanoic, and heptanoic acids; either octanol or pure water were used as control blanks. Most experiments were conducted using NA unless otherwise noted, as this acid was studied in the presence of photosensitizers [*Ciuraru et al*., 2015; *Rossignol et al*., 2016]. For

experiments aimed at detecting glyoxal, 3.5 mmol of the organic phase were injected onto the aqueous phase, corresponding to 615 μL, 555 μL, 495 μL, and 556 μL for NA, octanoic acid, heptanoic acid, and octanol respectively. If the organic compounds were fully dissolved in the aqueous phase, 3.5 mmol would correspond to 250 mmol L^{-1} solutions. However, the solubility of the organic compounds limits their concentration in the aqueous phase to 2–5 mmol L^{-1}. The remainder floated above the aqueous phase as a film and as distinct "islands." It was necessary to use these elevated concentrations to convert enough glyoxal precursors in the ozone reactor (see below), to ensure glyoxal detection. However, at these concentrations direct OVOC emissions saturate the gas phase analytical devices at the outlet of the reactor, such as the SRI-TOFMS. Therefore, experiments with the SRI-TOFMS used 5 and 10 mmol L^{-1} solutions of the corresponding acids.

2.3. Ozone Reactor

The ozone was generated by UV photolysis of oxygen (Stable Ozone Generator 1, Ultra-Violet Products Ltd., USA). The flow rate through the photoreactor into the ozone reactor was 300 mL min^{-1}. Air from the ozone generator added another 300 mL min^{-1} for a combined flow rate of 600 mL min^{-1} through the ozone reactor. The residence time of gas in the ozone reactor was approximately 8 min. Ozone concentrations were measured by LED-CE-DOAS and were approximately 0.5 ppmv. The rate constant for the reaction between *trans*-2-nonenal and ozone has been measured to be 2.05×10^{-18} cm^3 $molecule^{-1}$ s^{-1} [*Colmán et al.*, 2015]. At an ozone concentration of 0.5 ppmv (1.25×10^{13} molecule cm^{-3}), the quasi first-order reaction rate is 2.56×10^{-5} s^{-1}; only about 1% of the 2-nonenal is expected to react.

2.4. Time Protocol

A time protocol was established and followed for each experiment. For the first 20 min after the flow cell was filled and connected, the system was flushed with the ozone generator switched off and light from the xenon arc lamp blocked with a shutter. During this time, purified air continued to flow through the ozone generator to maintain a constant rate of flow throughout the entire experiment. The ozone generator was then turned on while the xenon arc lamp remained shuttered for 30 min. The shutter was opened and the photoreactor was irradiated for 2 h. Aluminum foil shielded the ozone reactor from UV irradiation. After the irradiation period, the shutter was closed on the xenon arc lamp while ozone continued to flow through the system for 1 h. Finally, the ozone generator was switched off, and the flow through the generator was increased to flush out the system for subsequent experiments.

2.5. Instrumentation and Detection

2.5.1. LED-CE-DOAS

Downstream of the ozone reactor, the air flowed through a T-connector to the LED-CE-DOAS, which was used to measure glyoxal before the air was exhausted. SRI-TOFMS could sample air in parallel with the LED-CE-DOAS from the T-connector. Briefly, a bright LED provides broadband light to an optical cavity. Mirror alignment was characterized by filling the cavity with reference gases such as nitrogen and helium, and comparing the observed scattering to the predicted Rayleigh scattering at different path lengths. The reflectivity of the mirrors at each wavelength could be measured and used to construct a reflectivity curve. Glyoxal was measured at a wavelength of 455 nm as described in *Coburn et al.* [2014], and was calibrated using the UV-vis spectrum by *Volkamer et al.* [2005]. At that wavelength, careful alignment of the mirrors provides path lengths of ~16 km, allowing detection of glyoxal at concentrations as low as several parts per trillion by volume (1 pptv = 10^{-12} volume mixing ratio = 2.46×10^7 molec cm^{-3}; 1 ppbv = 1000 pptv). Absorption by the O_2-O_2 (also termed O_4) collision complex allows for inherent calibration. For details of the operation of the University of Colorado LED-CE-DOAS refer to *Thalman and Volkamer* [2010]. The time resolution of the data collected by LED-CE-DOAS was approximately 1 min. The data were then averaged over 5 min.

2.5.2. SRI-TOFMS

A commercially available Selective Reagent Ionization Time-of-Flight Mass Spectrometer (SRI-TOFMS, Ionicon Analytik GmbH) using both H_3O^+ and NO^+ ionization modes was used to characterize gas phase products. The SRI-TOFMS system was mounted as shown Figure 1 to allow sampling both immediately downstream of the photoreactor and after the ozone reactor. The SRI-TOFMS inlet was connected to the Teflon system through 1.5 m of 6 mm ID PEEK tubing heated at 60°C. Measurements were performed at a drift voltage of 600 V, a drift temperature of 60°C and a drift pressure of 2.25 mbar resulting in an E/N of about 130–135 Td

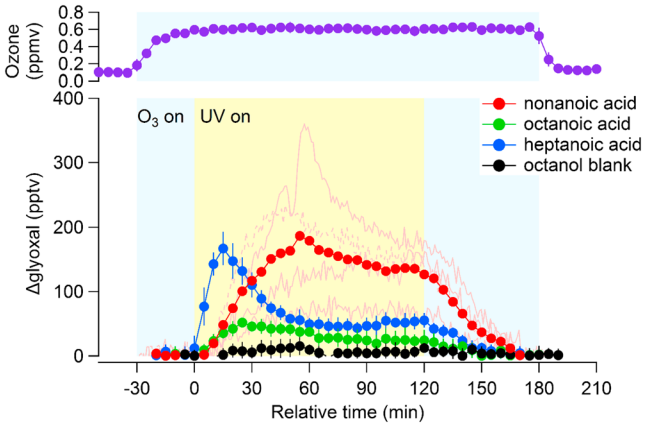

Figure 2. Time series of (top) ozone, and (bottom) background corrected glyoxal, both measured by LED-CE-DOAS. The traces are color coded for different organic compounds. Octanol (black line) was used as a blank. Each point is the average of all data collected using fresh and saltwater in a 5 min window. Error bars represent the standard deviations of the individual data points, and thin lines reflect individual experiments for NA. The dashed line represents a saltwater experiment.

($1\,\mathrm{Td} = 10^{-17}\,\mathrm{cm^2\,V^{-1}}$). The resolution of the spectra was approximately 4000 at m/z 100. More details concerning the different ionization modes are given in the supporting information.

2.6. Absorption Spectrum of NA

The UV absorption spectrum of a bulk solution of NA was measured using a Cary 5000 UV-vis-NIR spectrophotometer. Spectra were collected using quartz cuvettes with internal path lengths of 1.0, 4.0, 5.0, and 10.0 mm. The absorption spectrum was converted to an absorption cross section, and the four cross sections measured in this way were averaged in spectral ranges with sufficient signal-to-noise ratio (see Figure S2). Absorption spectra were also collected for solutions containing potassium biphthalate. Both an aqueous solution of $50\,\mathrm{mmol\,kg^{-1}}$ (buffer solution at pH = 4) and a saturated solution of potassium biphtalate in pure NA were used.

3. Results and Discussion

Figure 2 shows time traces of Δ-glyoxal, the background-corrected glyoxal, measured in experiments conducted with NA, octanoic acid, heptanoic acid, and octanol in the photoreactor. Figure 2 (top) shows a time trace of ozone measured by LED-CE-DOAS in a typical experiment. No significant glyoxal was observed when gas flows were started. Upon adding ozone in the dark some limited glyoxal (~50 pptv) was observed and is attributed to a memory effect in the Teflon tubing from previous experiments. This glyoxal background was characterized before and after each irradiation and typically varied by <10 pptv (see supporting information Table S1). A pronounced change in the glyoxal concentration was observed only upon irradiation of the photochemical reactor. Qualitatively similar results were observed for nonanoic, octanoic, and heptanoic acids, but not for octanol. We conclude that the formation of glyoxal is tied to the carboxylic acid functional group and is not observed for alcohols.

In the absence of ozone in the reaction chamber, the glyoxal concentrations were indistinguishable from zero when the simulated SML was irradiated. Experiments with only water and no organic phase in the photo reactor did not exhibit glyoxal production. These experiments had the ozone generator off for the entire time but used otherwise similar experimental conditions.

For all compounds, the time traces of glyoxal production were qualitatively very similar between fresh and saltwater. Therefore, the time traces for those compounds in Figure 2 display the averages of data from both fresh and saltwater experiments. With NA, the system exhibited significant variability and individual NA experiments are shown as thin pink lines, in addition to the 5 min average over the pooled data from all NA experiments. The Δ-glyoxal for individual experiments is given in Table S1 (supporting information). We hypothesize that the observed variability (factor 2 from the average Δ-glyoxal) is due to the formation of islands of excess fatty acid on the surface of the aqueous layer. A true monolayer of NA is expected to form at a concentration of about $0.6\,\mathrm{mmol\,L^{-1}}$ in our system. The unpredictable number, size, and location of such islands within the flow cell can cause irregular irradiation and chemical reactivity of the simulated SML due to scattering and refraction of the light and surface concentration effects. The partitioning of nonenal to tubing, coupled with the low reactivity of 2-nonenal with ozone and a desire for low glyoxal backgrounds requires elevated concentrations of NA to detect photochemical enhancements of glyoxal without limitations from backgrounds in our setup.

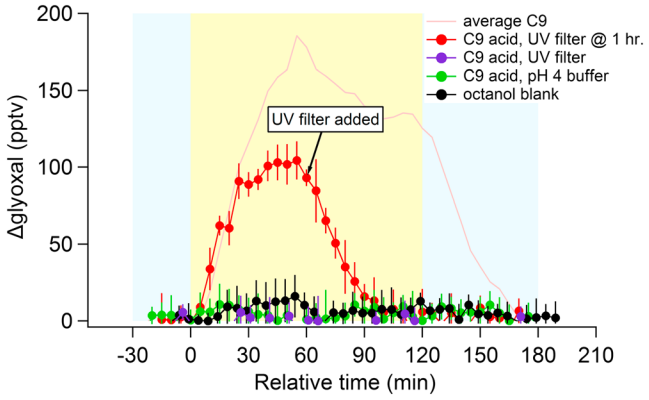

Figure 3. Time traces showing background-corrected glyoxal concentrations (Δ-glyoxal) in the LED-CE-DOAS as a function of time. The violet trace is the experiment in which a UV filter was introduced at the beginning of the experiment; the red trace has a UV filter introduced after 1 h. Error bars represent the standard deviations of data points in each 5 min average. For comparison, the light pink trace shows the average all NA fresh and saltwater experiments.

Time traces of Δ-glyoxal with NA in the presence of a UV filter with cutoff below 400 nm are shown in Figure 3. In the purple trace, a UV filter was placed between the xenon arc lamp and the photoreactor during the entire experiment. The Δ-glyoxal could not be distinguished from that of the octanol blank in that experiment. In the red trace, the UV glass filter was introduced only after 1 h of irradiation. In that experiment, the aqueous phase contained a 40 mg L^{-1} solution of humic acid, which has been used as a photosensitizer in previous work [*Ciuraru et al.*, 2015]. However, no photosensitizing effect was observed in our experiments; indeed, glyoxal concentrations in the presence of a photosensitizer were at the lower end of the glyoxal concentrations during experiments without humic acids. Glyoxal is initially produced, but after the glass filter is introduced, the glyoxal signal returns to the baseline, while visible wavelengths (>400 nm) continued to be present throughout the experiment. Therefore, the experiments using the UV glass filter indicate that the photoreactivity of the carboxylic acid can lead to the secondary formation of glyoxal only when irradiated with UV light.

Also shown in Figure 3 is the average time trace of two experiments in which the aqueous phase was a KHP pH 4 buffer solution. Conveniently, a pH 4 buffer does not substantially alter the pH of the aqueous phase below the floating NA; the pH of a NA-saturated subsurface aqueous phase was measured to be 3.9 in absence of pH buffer. KHP exhibits strong absorbance at wavelengths shorter than 310 nm and can therefore be used as an aqueous phase UV filter. The UV absorption spectrum of KHP is shown in Figure S1 (supporting information). Also shown are the transmission curves of such a solution for path lengths of 1, 5, and 10 cm. The transmission curves show that KHP prevents light <310 nm from reaching the vast majority the NA bulk phase or interface. In the pH = 4 buffer experiments, Δ-glyoxal was indistinguishable from the blank. Figure S1 also shows the UV absorption spectrum of NA (orange line) and NA saturated with KHP (green line). The increased absorption of light <300 nm indicates that some of the KHP partitions into neat NA solutions. However, no substantial change in the spectrum is observed at wavelengths >310 nm, indicating that the glyoxal suppression by KHP is not due to a change in the nature of the chromophore but could be due to limited UV transmission, or quenching of the excited state of NA. KHP is known to have a small quenching effect on fluorescence [*Williams and Bridges*, 1964] and could therefore chemically interact with the excited carboxylic function. However, such a quenching effect is likely of secondary importance here, because in our experiments the UV light cannot reach the NA in the first place (Figure S2).

During the experiments when SRI-TOFMS was connected, air was sampled both before and after the ozone reactor. In addition to using H_3O^+ as a reagent ion, we also used NO^+ to reduce fragmentation and obtain more selective information about the structural composition of the reaction products. Nonenal was observed to be the second most abundant unsaturated aldehyde present (the C_8 alkenal being the most abundant) before ozonolysis assigned based on the peak m/z 139.1117, corresponding to the $C_9H_{15}O^+$ ion in the NO^+ ionization mode (more details in the supporting information). Net production of 6–7 ppbv of nonenal was measured directly behind the photoreactor for experiments that use 5 mmol L^{-1} NA films in the absence of a photosensitizer, as shown Figure S3. This is broadly consistent with results described in [*Ciuraru et al.*, 2015], where a photosensitizer was present. The production rate of nonenal is 1–2 orders of magnitude larger than that of glyoxal, as is expected due to the limited residence time in the ozone reaction vessel. Heptanal was observed in small concentrations of 1–2 ppbv after the ozone reactor, although no significant concentration could be detected before ozonolysis. Broadly speaking, these results indicate that heptanal and glyoxal

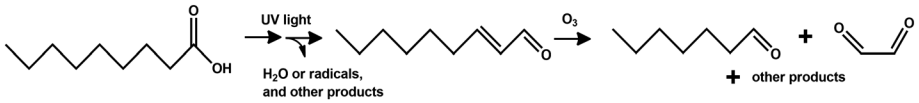

Figure 4. Proposed mechanism for secondary glyoxal production from carboxylic acids. In the first step, the carboxylic acid is transformed by photochemistry into 2-nonenal. In the second step, the 2-nonenal is cleaved by ozonolysis into glyoxal, an aliphatic aldehyde, and other products.

likely form as coproducts from the ozonolysis of 2-nonenal. The SRI-TOFMS data qualitatively show the production of other VOCs and OVOCs, confirming that the formation of 2-nonenal is only one branch of a rich product distribution. This is illustrated in Figure S3 by the time traces for a saturated aldehyde (octanal) and two unsaturated aldehydes (nonenal and propenal). Other unsaturated aldehydes could also contribute to the formation of glyoxal, either directly if its double bond is situated on carbon 2, or indirectly through a malondialdehyde intermediate if its double bond is situated on carbon 3 [*Zhou et al.*, 2014]. We propose a reaction mechanism whereby carboxylic acids photoexcitation by UV photons can eliminate water and form unsaturated OVOC including 2-nonenal that volatilize from the surface film, see Figure 4, and subsequently react with ozone in our system. The formation of 2-nonenal has been proposed to form OH radicals via a homolytic cleavage initiation pathway [*Rossignol et al.*, 2016]. Our results show that at least a fraction of the nonenal forms as 2-nonenal and thus provide evidence that the homolytic cleavage pathway is operative. Fatty acid films on the water interface absorb UV photons in the actinic flux region and undergo rapid photochemistry that is a source of HO_x radicals, unsaturated OVOC that form secondary glyoxal, and other aldehydes, even in the absence of a photosensitizer.

The action spectrum of NA was calculated as the product of the photon irradiance (photons $cm^{-2}\,nm^{-1}\,s^{-1}$) and the absorption cross section of NA (cm^2 $molecule^{-1}$; see Figure S2 in the supporting information), with the photochemically active wavelength range constrained to a very narrow region between 280 and 310 nm. The integral from 280 to 310 nm gives a J value of $3\times10^{-8}\,s^{-1}$ for NA in our experiments. The actual J value may be lower, if islands of NA were casting a shadow. Indeed, the glyoxal increased by a factor of 2 when NA islands were dispersed by shaking the photoreactor, though this effect could potentially also be explained by outgassing or by an increase of the interfacial surface. At a representative glyoxal volume mixing ratio of 200 pptv observed by LED-CE-DOAS, and a flow rate of 600 mL min^{-1}, the glyoxal production rate is 5×10^{10} molecules s^{-1}. The ratio of the glyoxal production rate to the NA photoexcitation rate is 8×10^{-4}. Considering further that only 1% of the nonenal will have time to react in the ozone reactor (see section 2.3), this suggests a quantum yield leading to nonenal of 8%. This estimate of the quantum yield is a lower limit, since the glyoxal yield from the ozonolysis could be smaller than unity, or because other reaction pathways that follow the photoexcitation do not result in nonenal formation.

4. Atmospheric Implications

Carboxylic acids are considered to be relatively unreactive in the atmosphere. The primary pathway consists of OH radical reactions that can give rise to decarboxylation [*Jenkin et al.*, 2003; *Saunders et al.*, 2003], or visible light overtone pumping [*Takahashi et al.*, 2008]. These processes are rather slow, resulting in atmospheric lifetimes of several days to a week with respect to oxidation; deposition is a major removal pathway for acids [*Keene et al.*, 2015]. By contrast, unsaturated aldehydes, such as 2-nonenal, are highly reactive. The reaction rate for the reaction of nonenal with OH radicals is 4.35×10^{-11} cm^3 $molecule^{-1}\,s^{-1}$ [*Gao et al.*, 2009], 2.05×10^{-18} cm^3 $molecule^{-1}\,s^{-1}$ for O_3 [*Colmán et al.*, 2015], and the kinetics of bromine atoms and photolysis remain unstudied (taken as that of methacrolein [*Calvert et al.*, 2015] for further discussion). Assuming concentrations of $[OH]=4\times10^6$ molecules cm^{-3}, $[Br]=2.5\times10^6$ molecules cm^{-3}, $[Cl]=5\times10^4$ molecules cm^{-3}, $J=6.6\times10^{-6}\,s^{-1}$, and $[O_3]=20$ ppbv (typical of the daytime remote marine boundary layer, MBL, in the tropics) the atmospheric lifetime of 2-nonenal is ~1 h. The atmospheric fate of 2-nonenal is determined by reaction with OH (67%), Br (25%), Cl (5%), and to a lesser extent by photolysis (2.6%) and O_3 (0.4%). Not only are unsaturated OVOC glyoxal precursors, they also appear to be a significant sinks for Br and Cl atoms in the MBL. Notably, air masses containing elevated glyoxal concentrations over oceans [*Sinreich et al.*, 2010; *Coburn et al.*, 2014; *Volkamer et al.*, 2015] also contain low BrO (upper limits <0.5 pptv) [*Gómez Martín et al.*, 2013; *Volkamer et al.*, 2015; *Wang et al.*, 2015]. This is despite the fact that sea spray aerosols

are acidic in the same air masses [*Miyazaki et al*., 2016]. This low BrO is incompatible with the fact that acidic aerosols liberate bromide efficiently [*Fickert et al*., 1999], and models predict higher BrO [*Long et al*., 2014; *Sherwen et al*., 2016]. A bromine sink from unsaturated OVOC in the marine MBL is currently not represented in atmospheric models [*Long et al*., 2014; *Sherwen et al*., 2016], in part due to the lack of kinetic data and product studies of the OH and Br radical reactions of unsaturated OVOC larger than C_4 [*Calvert et al*., 2015]. The lack of our understanding of marine OVOC emissions has the potential to bias our perception of halogen sources in the remote MBL.

Our results help explain a key feature of the missing source of glyoxal over oceans, where eddy covariance flux measurements indicate that the daytime flux is directed from the atmosphere into the ocean [*Coburn et al*., 2014]. Photochemical processes of DOC at the ocean surface liberate relatively low solubility VOCs to the atmosphere. Our results further indicate that photosensitizers [*Ciuraru et al*., 2015] are not needed to form unsaturated VOCs of low solubility from a variety of fatty acids. The subsequent oxidation of these VOCs in the marine atmosphere leads to secondary glyoxal. Due to the very high solubility of glyoxal and the vast undersaturation of glyoxal at the surface ocean, the net air-sea glyoxal flux is typically directed from the atmosphere into the ocean.

Previous field observations have reported widespread glyoxal in the MBL [*Zhou and Mopper*, 1990; *Sinreich et al*., 2010; *Mahajan et al*., 2014; *Coburn et al*., 2014; *Lawson et al*., 2015; *Volkamer et al*., 2015], with typical concentrations ranging from 7 to 80 pptv. Scaling our results to the atmosphere is subject to significant uncertainty, e.g., assumes all nonenal forms as 2-nonenal. The production rate of nonenal is 3×10^9 molecules cm^{-3} s^{-1} cm^{-2} in our setup (for 5 mmol L^{-1} NA) and presents the rate limiting step for the formation of secondary OVOCs. If we assume an effective yield of 10% or 100% glyoxal for all atmospheric reactions of 2-nonenal, and ~3 h glyoxal lifetime, the surface source can explain 3 to 30 pptv glyoxal throughout a 500 m deep boundary layer. In principle, acids could provide a significant fraction of the missing glyoxal source over oceans.

Future work is needed to establish the carbon balance, effective quantum yields, and molecular identify of acid photochemical products in the gas and condensed phases [*Rossignol et al*., 2016]. Surprisingly, high deposition fluxes of acids have been measured in the marine atmosphere [*Keene et al*., 2015], and their sources and fate in remote air are currently not well understood. Further, the chemical kinetics and products of the gas phase reaction of alkenals (larger C_4) with OH, Br, and Cl radicals and ozone are currently unstudied [*Calvert et al*., 2015]. The relative importance of these atmospheric oxidants is expected to vary between different isomers (e.g., 2- or 3-alkenals) and will be different in remote pristine and polluted marine air. Laboratory studies need to establish the reaction mechanisms of acids at interfaces and understand the identity of products and their fates in order to include this novel chemistry into atmospheric models.

Analytical challenges for the atmospheric detection of alkenal-type precursors arise from chemical complexity. Different acid molecules form a variety of precursor molecules that all contribute some glyoxal (and different OVOC). Furthermore, the atmospheric lifetime of glyoxal is significantly longer (several hours) compared to 2-alkenal-type species leading to the expectation of extremely low concentrations of individual precursor molecules. This may be the reason that the glyoxal source over oceans remains elusive to date [*Mopper and Zhou*, 1990; *Sinreich et al*., 2010; *Lawson et al*., 2015]. The relevance of acids as a secondary source of glyoxal may not be limited to the marine atmosphere. Atmospheric models currently explain only about 50% of the global terrestrial source of glyoxal. The largest model-satellite mismatch is observed over biogenic hot spots where acids and isoprene are abundant such as the Amazon rain forest [*Stavrakou et al*., 2009] and over remote oceans [*Myriokefalitakis et al*., 2008]. The global glyoxal source (~128 Tg yr^{-1}) warrants reexamination. The presence of glyoxal in the free troposphere over the South Eastern U.S. [*Lee et al*., 1998], over Los Angeles [*Baidar et al*., 2013], and over the tropical Eastern Pacific Ocean [*Volkamer et al*., 2015] is further surprising and may point to shortcomings in our understanding of the biogeochemical cycle of organic carbon. Acids are widespread over continents and oceans [*Keene et al*., 2015], and missing sources of glyoxal in atmospheric models have implications for secondary organic aerosol formation [*Volkamer et al*., 2007; *Fu et al*., 2008; *Washenfelder et al*., 2011; *Rinaldi et al*., 2011; *Waxman et al*., 2013; *Knote et al*., 2014].

Acknowledgments

This study was supported by U.S. National Science Foundation in form of a CAREER award Supplement (NSF-ATM-847793) to facilitate collaboration with the European Research Council under the European Union's Seventh Framework Program (FP/2007-2013)/ERC grant agreement 290852–AIRSEA. L. G. acknowledges a Chateaubriand fellowship from the French embassy in the U.S. RC acknowledges travel funds from NSF-EAGER award AGS-1452317. The authors are grateful to Nicolas Charbonnel and Sebastien Perrier for the technical support provided. The data displayed in graphs are available from the following data archive: http://ciresgroups.colorado.edu/volkamergroup/index.php/publications.

References

Baidar, S., H. Oetjen, S. Coburn, B. Dix, I. Ortega, R. Sinreich, and R. Volkamer (2013), The CU Airborne MAX-DOAS instrument: Vertical profiling of aerosol extinction and trace gases, *Atmos. Meas. Tech*., *6*(3), 719–739, doi:10.5194/amt-6-719-2013.

Calvert, J. G., J. J. Orlando, W. R. Stockwell, and T. J. Wallington (2015), *The Mechanisms of Reactions Influencing Atmospheric Ozone*, Oxford Univ. Press, New York.

Ciuraru, R., L. Fine, M. van Pinxteren, B. D'Anna, H. Herrmann, and C. George (2015), Photosensitized production of functionalized and unsaturated organic compounds at the air-sea interface, *Sci. Rep.*, *5*, 12741, doi:10.1038/srep12741.

Coburn, S., I. Ortega, R. Thalman, B. Blomquist, C. W. Fairall, and R. Volkamer (2014), Measurements of diurnal variations and eddy covariance (EC) fluxes of glyoxal in the tropical marine boundary layer: Description of the Fast LED-CE-DOAS instrument, *Atmos. Meas. Tech.*, *7*(10), 3579–3595, doi:10.5194/amt-7-3579-2014.

Colmán, E. G., M. B. Blanco, I. Barnes, and M. A. Teruel (2015), Ozonolysis of a series of C7–C9 unsaturated biogenic aldehydes: Reactivity study at atmospheric pressure, *RSC Adv.*, *5*(39), 30,500–30,506, doi:10.1039/C4RA17283C.

Fickert, S., J. W. Adams, and J. N. Crowley (1999), Activation of Br_2 and BrCl via uptake of HOBr onto aqueous salt solutions, *J. Geophys. Res.*, *104*, 23,719–23,727, doi:10.1029/1999JD900359.

Fu, T.-M., D. J. Jacob, F. Wittrock, J. P. Burrows, M. Vrekoussis, and D. K. Henze (2008), Global budgets of atmospheric glyoxal and methylglyoxal, and implications for formation of secondary organic aerosols, *J. Geophys. Res.*, *113*, D15303, doi:10.1029/2007JD009505.

Gantt, B., N. Meskhidze, and D. Kamykowski (2009), A new physically-based quantification of marine isoprene and primary organic aerosol emissions, *Atmos. Chem. Phys.*, *9*(14), 4915–4927, doi:10.5194/acp-9-4915-2009.

Gao, T., J. M. Andino, C. C. Rivera, and M. F. Márquez (2009), Rate constants of the gas-phase reactions of OH radicals with *trans*−2-hexenal, *trans*−2-octenal, and *trans*−2-nonenal, *Int. J. Chem. Kinet.*, *41*(7), 483–489, doi:10.1002/kin.20424.

Gómez Martín, J. C., et al. (2013), Iodine chemistry in the eastern Pacific marine boundary layer, *J. Geophys. Res. Atmos.*, *118*, 887–904, doi:10.1002/jgrd.50132.

Hawkins, L. N., L. M. Russell, D. S. Covert, P. K. Quinn, and T. S. Bates (2010), Carboxylic acids, sulfates, and organosulfates in processed continental organic aerosol over the southeast Pacific Ocean during VOCALS-REx 2008, *J. Geophys. Res.*, *115*, D13201, doi:10.1029/2009JD013276.

Ip, H. S. S., X. H. H. Huang, and J. Z. Yu (2009), Effective Henry's law constants of glyoxal, glyoxylic acid, and glycolic acid, *Geophys. Res. Lett.*, *36*, L01802, doi:10.1029/2008GL036212.

Jenkin, M. E., S. M. Saunders, V. Wagner, and M. J. Pilling (2003), Protocol for the development of the Master Chemical Mechanism, MCM v3 (Part B): Tropospheric degradation of aromatic volatile organic compounds, *Atmos. Chem. Phys.*, *3*, 181–193.

Kampf, C. J., E. M. Waxman, J. G. Slowik, J. Dommen, L. Pfaffenberger, A. P. Praplan, A. S. H. Prévoît, U. Baltensperger, T. Hoffmann, and R. Volkamer (2013), Effective Henry's law partitioning and the salting constant of glyoxal in aerosols containing sulfate, *Environ. Sci. Technol.*, *47*(9), 4236–4244, doi:10.1021/es400083d.

Kawamura, K., K. Ono, E. Tachibana, B. Charriére, and R. Sempéré (2012), Distributions of low molecular weight dicarboxylic acids, ketoacids and α-dicarbonyls in the marine aerosols collected over the Arctic Ocean during late summer, *Biogeosciences*, *9*, 4725–4737, doi:10.5194/bg-9-4725-2012.

Keene, W. C., J. N. Galloway, G. E. Likens, F. A. Deviney, K. N. Mikkelsen, J. L. Moody, and J. R. Maben (2015), Atmospheric wet deposition in remote regions: Benchmarks for environmental change, *J. Atmos. Sci.*, *72*(8), 2947–2978, doi:10.1175/JAS-D-14-0378.1.

Kieber, D. J., J. McDaniel, and K. Mopper (1989), Photochemical source of biological substrates in sea water: Implications for carbon cycling, *Nature*, *341*(6243), 637–639, doi:10.1038/341637a0.

Kieber, D. J., W. C. Keene, A. A. Frossard, M. S. Long, J. R. Maben, L. M. Russell, J. D. Kinsey, I. M. B. Tyssebotn, P. K. Quinn, and T. S. Bates (2016), Coupled ocean-atmosphere loss of marine refractory dissolved organic carbon, *Geophys. Res. Lett.*, *43*, 2765–2772, doi:10.1002/2016GL068273.

Kieber, R. J., X. Zhou, and K. Mopper (1990), Formation of carbonyl compounds from UV-induced photodegradation of humic substances in natural waters: Fate of riverine carbon in the sea, *Limnol. Oceanogr.*, *35*(7), 1503–1515, doi:10.4319/lo.1990.35.7.1503.

King, M. D., A. R. Rennie, K. C. Thompson, F. N. Fisher, C. C. Dong, R. K. Thomas, C. Pfrang, and A. V. Hughes (2009), Oxidation of oleic acid at the air–water interface and its potential effects on cloud critical supersaturations, *Phys. Chem. Chem. Phys.*, *11*, 7699–7707, doi:10.1039/b906517b.

Knote, C., et al. (2014), Simulation of semi-explicit mechanisms of SOA formation from glyoxal in aerosol in a 3-D model, *Atmos. Chem. Phys.*, *14*, 6213–6239, doi:10.5194/acp-14-6213-2014.

Lawson, S. J., P. W. Selleck, I. E. Galbally, M. D. Keywood, M. J. Harvey, C. Lerot, D. Helmig, and Z. Ristovski (2015), Seasonal in situ observations of glyoxal and methylglyoxal over the temperate oceans of the Southern Hemisphere, *Atmos. Chem. Phys.*, *15*, 223–240, doi:10.5194/acp-15-223-2015.

Lee, Y.-N., et al. (1998), Atmospheric chemistry and distribution of formaldehyde and several multioxygenated carbonyl compounds during the 1995 Nashville/Middle Tennessee Ozone Study, *J. Geophys. Res.*, *103*, 22,449–22,462, doi:10.1029/98JD01251.

Lerot, C., T. Stavrakou, I. De Smedt, J.-F. Müller, and M. Van Roozendael (2010), Glyoxal vertical columns from GOME-2 backscattered light measurements and comparisons with a global model, *Atmos. Chem. Phys.*, *10*(24), 12,059–12,072, doi:10.5194/acp-10-12059-2010.

Liss, P. S., and R. A. Duce (1997), *The Sea Surface and Global Change*, Cambridge Univ. Press, Cambridge, U. K.

Long, M. S., W. C. Keene, D. J. Kieber, A. A. Frossard, L. M. Russell, J. R. Maben, J. D. Kinsey, P. K. Quinn, and T. S. Bates (2014), Light-enhanced primary marine aerosol production from biologically productive seawater, *Geophys. Res. Lett.*, *41*, 2661–2670, doi:10.1002/2014GL059436.

Mahajan, A. S., et al. (2014), Glyoxal observations in the global marine boundary layer, *J. Geophys. Res. Atmos.*, *119*, 6160–6169, doi:10.1002/2013JD021388.

Millet, D. B., et al. (2010), Global atmospheric budget of acetaldehyde: 3-D model analysis and constraints from in-situ and satellite observations, *Atmos. Chem. Phys.*, *10*(7), 3405–3425, doi:10.5194/acp-10-3405-2010.

Miyazaki, Y., S. Coburn, K. Ono, D. T. Ho, R. B. Pierce, K. Kawamura, and R. Volkamer (2016), Contribution of dissolved organic matter to submicron water-soluble organic aerosols in the marine boundary layer over the eastern equatorial Pacific, *Atmos. Chem. Phys. Discuss.*, *16*, 7695–7707, doi:10.5194/acp-2016-164.

Mopper, K., and X. Zhou (1990), Hydroxyl radical photoproduction in the sea and its potential impact on marine processes, *Science*, *250*(4981), 661–664, doi:10.1126/science.250.4981.661.

Mopper, K., X. Zhou, R. J. Kieber, D. J. Kieber, R. J. Sikorski, and R. D. Jones (1991), Photochemical degradation of dissolved organic carbon and its impact on the oceanic carbon cycle, *Nature*, *353*(6339), 60–62, doi:10.1038/353060a0.

Moran, M. A., and R. G. Zepp (1997), Role of photoreactions in the formation of biologically labile compounds from dissolved organic matter, *Limnol. Ocermogr.*, *42*(6), 1307–1316.

Myriokefalitakis, S., M. Vrekoussis, K. Tsigaridis, F. Wittrock, A. Richter, C. Brühl, R. Volkamer, J. P. Burrows, and M. Kanakidou (2008), The influence of natural and anthropogenic secondary sources on the glyoxal global distribution, *Atmos. Chem. Phys. Discuss.*, *8*(2), 1673–1708, doi:10.5194/acpd-8-1673-2008.

O'Dowd, C. D., M. C. Facchini, F. Cavalli, D. Ceburnis, M. Mircea, S. Decesari, S. Fuzzi, Y. J. Yoon, and J.-P. Putaud (2004), Biogenically driven organic contribution to marine aerosol, *Nature*, *431*(7009), 676–680, doi:10.1038/nature02959.

Quinn, P. K., T. S. Bates, K. S. Schulz, D. J. Coffman, A. A. Frossard, L. M. Russell, W. C. Keene, and D. J. Kieber (2014), Contribution of sea surface carbon pool to organic matter enrichment in sea spray aerosol, *Nat. Geosci.*, *7*(3), 228–232, doi:10.1038/ngeo2092.

Rinaldi, M., et al. (2011), Evidence of a natural marine source of oxalic acid and a possible link to glyoxal, *J. Geophys. Res.*, *116*, D16204, doi:10.1029/2011JD015659.

Rossignol, S., L. Tinel, A. Bianco, M. Passananti, M. Brigante, D. J. Donaldson, and C. George (2016), Atmospheric photochemistry at a fatty acid-coated air-water interface, *Science*, *353*(6300), 699–702, doi:10.1126/science.aaf3617.

Saunders, S. M., M. E. Jenkin, R. G. Derwent, and M. J. Pilling (2003), Protocol for the development of the Master Chemical Mechanism, MCM v3 (Part A): Tropospheric degradation of non-aromatic volatile organic compounds, *Atmos. Chem. Phys.*, *3*(1), 161–180, doi:10.5194/acp-3-161-2003.

Sherwen, T., et al. (2016), Global impacts of tropospheric halogens (Cl, Br, I) on oxidants and composition in GEOS-Chem, *Atmos. Chem. Phys.*, *16*, 12,239–12,271, doi:10.5194/acp-2016-424.

Sinreich, R., S. Coburn, B. Dix, and R. Volkamer (2010), Ship-based detection of glyoxal over the remote tropical Pacific Ocean, *Atmos. Chem. Phys.*, *10*(23), 11,359–11,371, doi:10.5194/acp-10-11359-2010.

Spracklen, D. V., S. R. Arnold, J. Sciare, K. S. Carslaw, and C. Pio (2008), Globally significant oceanic source of organic carbon aerosol, *Geophys. Res. Lett*, *35*, L12811, doi:10.1029/2008GL033359.

Stavrakou, T., J.-F. Müller, I. De Smedt, M. Van Roozendael, M. Kanakidou, M. Vrekoussis, F. Wittrock, A. Richter, and J. P. Burrows (2009), The continental source of glyoxal estimated by the synergistic use of spaceborne measurements and inverse modelling, *Atmos. Chem. Phys.*, *9*(21), 8431–8446, doi:10.5194/acp-9-8431-2009.

Takahashi, K., K. L. Plath, R. T. Skodje, and V. Vaida (2008), Dynamics of vibrational overtone excited pyruvic acid in the gas phase: Line broadening through hydrogen-atom chattering, *J. Phys. Chem. A*, *112*(32), 7321–7331, doi:10.1021/jp803225c.

Thalman, R., and R. Volkamer (2010), Inherent calibration of a blue LED-CE-DOAS instrument to measure iodine oxide, glyoxal, methyl glyoxal, nitrogen dioxide, water vapour and aerosol extinction in open cavity mode, *Atmos. Meas. Tech*, *3*, 1797–1814, doi:10.5194/amt-3-1797-2010.

Turekian, V. C., S. A. Macko, and W. C. Keene (2003), Concentrations, isotopic compositions, and sources of size-resolved, particulate organic carbon and oxalate in near-surface marine air at Bermuda during spring, *J. Geophys. Res.*, *108*(D5), 4157, doi:10.1029/2002JD002053.

Volkamer, R., F. San Martini, L. T. Molina, D. Salcedo, J. L. Jimenez, and M. J. Molina (2007), A missing sink for gas-phase glyoxal in Mexico City: Formation of secondary organic aerosol, *Geophys. Res. Lett.*, *34*, L19807, doi:10.1029/2007GL030752.

Volkamer, R., et al. (2015), Aircraft measurements of BrO, IO, glyoxal, NO_2, H_2O, O_2–O_2 and aerosol extinction profiles in the tropics: Comparison with aircraft-/ship-based in situ and lidar measurements, *Atmos. Meas. Tech.*, *8*(5), 2121–2148, doi:10.5194/amt-8-2121-2015.

Volkamer, R., P. Spietz, J. H. Burrows, and U. Platt (2005), High-resolution absorption cross-section of glyoxal in the UV–vis and IR spectral ranges, *J. Photochem. Photobiol., A*, *172*(1), 35–46, doi:10.1016/j.jphotochem.2004.11.011.

Wang, S., et al. (2015), Active and widespread halogen chemistry in the tropical and subtropical free troposphere, *Proc. Natl. Acad. Sci. U.S.A.*, *112*(30), 9281–2986, doi:10.1073/pnas.1505142112.

Washenfelder, R. A., et al. (2011), The glyoxal budget and its contribution to organic aerosol for Los Angeles, California, during CalNex 2010, *J. Geophys. Res.*, *116*, D00V02, doi:10.1029/2011JD016314.

Waxman, E. M., J. Elm, T. Kurtén, K. V. Mikkelsen, P. J. Ziemann, and R. Volkamer (2015), Glyoxal and methylglyoxal setschenow salting constants in sulfate, nitrate, and chloride solutions: Measurements and Gibbs energies, *Environ. Sci. Technol.*, *49*(19), 11,500–11,508, doi:10.1021/acs.est.5b02782.

Waxman, E. M., K. Dzepina, B. Ervens, J. Lee-Taylor, B. Aumont, J. L. Jimenez, S. Madronich, and R. Volkamer (2013), Secondary organic aerosol formation from semi- and intermediate-volatility organic compounds and glyoxal: Relevance of O/C as a tracer for aqueous multiphase chemistry, *Geophys. Res. Lett.*, *40*, 978–982, doi:10.1002/grl.50203.

Williams, R. T., and J. W. Bridges (1964), Fluorescence of solutions: A review, *J. Clin. Pathol.*, *17*(1), 371–394, doi:10.1136/jcp.17.4.371.

Wittrock, F., A. Richter, H. Oetjen, J. P. Burrows, M. Kanakidou, S. Myriokefalitakis, R. Volkamer, S. Beirle, U. Platt, and T. Wagner (2006), Simultaneous global observations of glyoxal and formaldehyde from space, *Geophys. Res. Lett.*, *33*, L16804, doi:10.1029/2006GL026310.

Zahardis, J., and G. A. Petrucci (2007), The oleic acid-ozone heterogeneous reaction system: Products, kinetics, secondary chemistry, and atmospheric implications of a model system—A review, *Atmos. Chem. Phys.*, *7*, 1237–1274.

Zhou, X. L., and K. Mopper (1990), Apparent partition-coefficients of 15 carbonyl-compounds between air and seawater and between air and fresh-water—Implications for air sea exchange, *Environ. Sci. Technol.*, *24*, 1864–1869.

Zhou, S., et al. (2014), Formation of gas-phase carbonyls from heterogeneous oxidation of polyunsaturated fatty acids at the air–water interface and of the sea surface microlayer, *Atmos. Chem. Phys.*, *14*, 1371–1384, doi:10.5194/acp-14-1371-2014.